ARTICLES SCIENCE CHINA Materials

mater.scichina.com link.springer.com

Published online 25 October 2019 | https://doi.org/10.1007/s40843-019-1180-8

Sci China Mater 2020, 63(2): 276–287

Construction of layered h-BN/TiO_2 hetero-structure and probing of the synergetic photocatalytic effect

Qun Li[1], Xinmei Hou[1*], Zhi Fang[1], Tao Yang[1], Junhong Chen[2], Xiangzhi Cui[3*], Tongxiang Liang[4] and Jianlin Shi[3]

ABSTRACT **A novel layered hexagonal boron nitride/titanium dioxide (h-BN/TiO_2) composite photocatalyst has been constructed by anchoring TiO_2 nanoflakes on the surface of h-BN flakes *via* a solvothermal method. The morphology and dispersion of TiO_2 can be tuned by controlling the amount of flake h-BN. Benefiting from the unique hetero-structure, the photocatalytic performance of the obtained composite toward rhodamine B (RhB) degradation is greatly enhanced, among which 12 wt% h-BN/TiO_2 composites show 3.5 and 6.9 times higher degradation rate than the synthesized TiO_2 and commercial TiO_2 (P25), respectively, and an excellent cycling stability has also been obtained. Moreover, the first-principles calculation reveals the synergetic catalytic effect between TiO_2 and h-BN flake, which is found to be responsible for the significantly enhanced photocatalytic performance of h-BN/TiO_2 composites.**

Keywords: layered nanostructure, h-BN flake, TiO_2 nanoflake, photocatalytic activity, dye degradation

INTRODUCTION

Photocatalytic degradation has increasingly become one of the effective approaches for solving environmental pollution by decomposing toxic complex organic pollutants into less toxic or even completely harmless molecules under sunlight or UV illumination [1]. Among the various semiconductor photocatalysts, titanium dioxide (TiO_2) has fostered considerable interest in organic dye degradation due to its high efficiency, low cost, non-toxicity and chemical stability [2,3]. However, owing to low utilization efficiency of sunlight (about 4%) and the fast recombination of photogenerated electrons and holes, bare TiO_2 exhibits low photocatalytic efficiency, which greatly limits its practical use [4]. Nowadays, two strategies are usually developed to enhance the photocatalytic activity. One is to decrease the size and design unique structure to promote the mobility and separation of photogenerated electrons and holes [5]. The other is to combine semiconductors with other favorable materials to construct semiconductor-based heterostructures and composite systems for visible-light-driven light harvesting systems [6,7]. To sum up, developing a composite system with a controllable structure by combining the above two advantages has profound meaning.

Hexagonal boron nitride (h-BN), with a two dimensional (2D) graphite-like structure, has opened up a new frontier in materials for the development of clean and renewable energy conversion and energy storage systems on account of high chemical stability, high thermal stability, low density, biocompatibility and environmental friendliness [8,9]. To our knowledge, h-BN is commonly excluded in photocatalysis and photovoltaic conversion applications due to its wide gap [10]. However, recent studies have proved the feasibility of h-BN as catalyst support materials to effectively enhance the photocatalytic properties of semiconductor materials because of the interactions between them, for instance, SnO_2/h-BN submicro-boxes (BNMB) [11], BN/Ag_2CO_3 [12], h-BN/$Bi_4O_5Br_2$-layered microspheres [13], CdS/BN nanosheets (BNNSs) [14], BN/AgBr [15] and BN/$Bi_4O_5I_2$ [16]. The enhancement of photocatalytic propeties is generally ascribed to the suppressed recombination of photogenerated electrons and holes, extended excitation wavelength and increased amount of surface-adsorbed

[1] Collaborative Innovation Center of Steel Technology, University of Science and Technology Beijing, Beijing 100083, China
[2] School of Material Science and Technology, University of Science and Technology Beijing, Beijing 100083, China
[3] The State Key Laboratory of High Performance Ceramics and Superfine Microstructures, Shanghai Institute of Ceramics, Chinese Academy of Sciences, Shanghai 200050, China
[4] School of Materials Science and Engineering, Jiangxi University of Science and Technology, Ganzhou 341000, China
[*] Corresponding authors (emails: houxinmeiustb@ustb.edu.cn (Hou X); cuixz@mail.sic.ac.cn (Cui X))

reactant [17]. However, the role of h-BN in the photocatalytic enhancement of the composites is still under debate. Furthermore, from the aforementioned BN-semiconductor composites, it can be found that the photocatalytic properties are largely determined by the morphology of the semiconductors and support materials [18,19]. In this work, layered h-BN/TiO_2 composites with flake-on-flake hetero-structure are constructed and expected to improve photocatalytic activities. Multiple techniques including X-ray diffraction (XRD), scanning electron microscopy (SEM), transmission electron microscopy (TEM) and X-ray photoelectron spectroscopy (XPS) were used to characterize the obtained composites. The effect of the flake h-BN on the photocatalytic performance of the composites was investigated by degrading rhodamine B (RhB) under visible light irradiation. Moreover, the possible mechanism for the improved photocatalytic activity was discussed in detail by the first-principles calculation.

EXPERIMENTAL SECTION

Preparation of flake h-BN

All the chemicals used in this research were of analytical purity and without further purification prior to use. The synthesis of the h-BN was reported in our previous paper [20]. Typically, the foamy precursor was prepared by low temperature combustion synthesis (LCS) method in air in a muffle furnace using H_3BO_3, $C_6H_{12}O_6{\cdot}H_2O$, $CO(NH_2)_2$ and HNO_3 as raw materials. Then, h-BN was obtained by calcining the foamy precursor at 900°C for 3 h in flowing NH_3. The residual carbon and B_2O_3 were removed by annealing in air and washing with hot water, respectively.

Preparation of h-BN/TiO_2 composites

The h-BN/TiO_2 composites with different contents of h-BN were prepared by a simple solvothermal process. Typically, 1 mL $TiCl_3$ and 1 mL deionized water were added into 30 mL of ethylene glycol under stirring to produce a light purple solution. Then, a certain amount of h-BN was suspended in the mixed solution, which was put into a 50-mL Teflon-lined stainless steel autoclave. The sealed autoclave was heated at 150°C for 12 h and then cooled naturally to room temperature. The as-obtained products were centrifuged, washed with ethanol several times and dried at room temperature. Finally, the products were annealed at 350°C for 2 h to remove all organic species adsorbed on the composites and improve the crystallinity at the same time. The obtained samples were named as *X* wt% h-BN/TiO_2, where *X* was the mass fraction of h-BN during the synthetic process. For comparison, TiO_2 was synthesized by the similar method without addition of h-BN.

Characterization

The phase of the obtained samples was firstly examined by XRD (M21XVHF22, MAC Science, Yokohama, Japan) with a TTRIII diffractometer equipped with Cu Kα radiation over a 2θ range from 10° to 90°. The morphology and surface roughness of the obtained samples were observed by cold field emission SEM (FE-SEM, ZEISS SUPRATM 55, Germany). TEM (HITACHI H8100, Hitachi, Japan) was used to further investigate the microstructure. High resolution TEM (HRTEM, JEM 2010, Joel Ltd. Japan) was used to characterize the phase and crystal morphology of the products. The specific surface area was determined from the nitrogen adsorption-desorption isotherm measured at 77 K on Quadrasorb SI-MP analyzer using Brunauer-Emmett-Teller (BET) model. The chemical states of the composites were determined by XPS. The optical properties of the samples were analyzed by UV-Vis spectrophotometer (UV2250, Shimadzu), in which $BaSO_4$ was used as the reflectance standard material. Photoluminescence (PL) emission spectra were measured on a Hitachi F-7000 fluorescence spectrophotometer at an excitation wavelength of 361 nm.

Photoelectrochemical measurement

The indium tin oxide (ITO) glass with an area of 1 × 2 cm^2 was washed ultrasonically in acetone and ethanol for a few minutes, respectively. The cleaned ITO glass was dried for the next modification. The h-BN/TiO_2 composites and polyvinylidene fluoride (PVDF) with the mass ratio of 95:5 were dispersed in *N*-methyl-2-pyrrolidone (NMP) to form a stable suspension, and then the suspension was deposited on the ITO glass with an area of 1 × 1 cm^2. Finally, the modified ITO glass was heated at 60°C overnight to evaporate the solvent for the photoelectrochemical measurement, which was tested in 0.2 mol L^{-1} Na_2SO_4 solution on a CHI660D electrochemical working station consisting of an Ag/AgCl reference electrode, a platinum wire counter electrode, and a modified ITO glass working electrode. The photocurrent *vs.* irradiation time curve was recorded at 0 V under dark (20 s) and light (20 s), respectively. A light source used in the work was a 300 W Xe lamp with a 400 nm cut-off filter and the light intensity density was 100 mW cm^{-2}.

Photocatalytic performance of the as-prepared sample

Photocatalytic performance of the h-BN/TiO_2 composites was evaluated by irradiating 20 mL RhB (10 mg L^{-1}) and phenol (40 mg L^{-1}) in the presence of 0.75 g L^{-1} h-BN/TiO_2 under stirring. Before irradiation, the suspension was magnetically stirred for 30 min to achieve adsorption-desorption equilibrium. During the irradiation process, 5 mL of the suspension was collected and centrifuged to obtain supernatant. The concentration of RhB and phenol was examined at different time intervals by UV-vis spectrophotometer at 554 and 269 nm, respectively. The degradation efficiency was calculated by the following expression [21]:

$$\text{Efficiency} = \frac{C_t}{C_0}, \quad (1)$$

where C_0 is the initial concentration of RhB and phenol solution; C_t is the concentration at given test time.

First-principles calculations

All calculations were performed by density functional theory (DFT) using the Perdew-Burke-Ernzerhof (PBE) functional [22], as implemented in Vienna *ab-initio* Simulation Package (VASP) [23]. Electron-ion interactions were described by the projector-augmented wave (PAW) potentials with a kinetic energy cutoff of 450 eV [24]. The valence electron configurations for Ti, O, B, N, C, and H were $3p^6 3p^2 4s^2$, $2s^2 2p^4$, $2s^2 2p^1$, $2s^2 2p^3$, $2s^2 2p^2$ and $1s^1$, respectively. To correct the self-interaction error, the DFT +U method was adopted, where a Hubbard-type correction was applied on the 3d orbitals of Ti and 2p orbitals of O [25]. Effective U = 4.2 eV for Ti 3d and U = 6.3 eV for O 2p orbitals were selected on the basis of previous work [26], which provided a correct description of the polaronic states of TiO_2. The structure relaxation was stopped when the force on each atom was below 0.05 eV/Å.

The anatase TiO_2 (101) surface was modeled by 4×1 periodically repeated slabs and a four-layered model was used (Fig. S1a). A 20 Å vacuum was added between slabs along the [101] direction to simulate the open surface. One layered h-BN was combined with TiO_2 slab to model h-BN/TiO_2 composites (Fig. S1b). The lattice mismatch was smaller than 5% and the distance between these two slabs has been optimized. A Monkhorst-Pack grid of 6×2×1 k points mesh centered at the Γ point was used for all DFT calculations. Electronic band structure and density of state (DOS) were calculated to analyze the contribution of h-BN to photocatalysis. Adsorption energies of organic molecules were applied to evaluate the adsorption capacity of photocatalysts and the charge-density difference was used to study the charge transfer between h-BN and TiO_2. Electron effective masses (m_e^*) and hole effective masses (m_h^*) were calculated by the method of parabolic band fitting around the conduction band minimum (CBM) or the valence band maximum (VBM) according to the following equations:

$$(m^*)_{ij} = \hbar^2 \left[\frac{\partial \varepsilon_n \vec{k}}{\partial k_i k_j} \right]^{-1}, i,j = x,y,z, \quad (2)$$

where m^* is the effective mass of the charge carrier, i and j denote reciprocal components, $\varepsilon_n \vec{k}$ is the energy dispersion function of the nth band, $\vec{k}$ is the wave vector, and $\hbar$ represents the reduced Planck constant. For better fitting parabolic within the VBM and CBM regions, the non-self-consistent calculation for band structure was performed using 61 k-points around VBM or CBM with a separation of 0.002 $Å^{-1}$.

In addition, the adsorption energies of RhB on photocatalysts were calculated to evaluate their adsorption ability. Because RhB molecule is so huge that the surface of slabs would be very large and the calculation would be quite time-consuming. Besides, de-ethylation of RhB is one of the most important steps during the degradation process. Two different parts of the RhB with ethyl groups were chosen as the adsorbed molecules.

RESULTS AND DISCUSSION

Fig. 1 shows the XRD patterns of h-BN, TiO_2 and the annealed h-BN/TiO_2 with different h-BN contents. As for h-BN, two broad diffraction peaks at 2θ=20°–30° and 40°–45° can be indexed to the (002) and (100) facets of h-BN (PDF 34-421), respectively. For TiO_2, before calci-

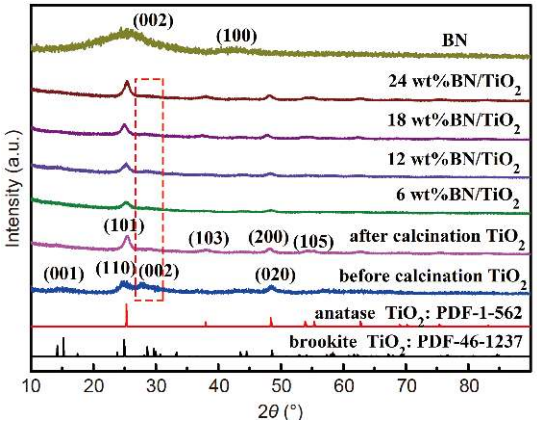

Figure 1 The XRD patterns of h-BN, TiO_2 and h-BN/TiO_2 samples with different contents of flake h-BN.

nation, it can be clearly found that the peaks for (001), (110), (002) and (020) correspond to the TiO_2 brookite (B) crystalline phase (PDF 46-1237) [27]. However, after calcination, the phase of the TiO_2 gradually transforms from brookite to anatase crystalline phase (PDF 1-562). Interestingly, the phase transformation is not complete, which leads to the enhancement of the photocatalytic activity of TiO_2 due to the existence of two crystal structures acting as semiconductor heterojunction [28]. After h-BN was introduced, all diffraction peaks of the obtained h-BN/TiO_2 composites can be clearly indexed to anatase TiO_2 crystals except for the (002) small peak of the brookite phase (marked by the red line). And no distinct diffraction peaks of h-BN can be observed due to dense TiO_2 covering on its surface.

The effect of the flake h-BN content on the TiO_2 microstructure was also investigated and shown in Fig. S2. Fig. S2a and b indicate that pure TiO_2 assembled from 2D nanoflakes has a hierarchical microsphere structure with an average diameter of 200 nm. After the flake h-BN is introduced, the structure of TiO_2 gradually transforms from microsphere into randomly oriented nanoflakes and nano grasses structure has been formed with the increase of the addition of flake h-BN (Fig. S2c–j). The result reveals that the morphology and dispersion of TiO_2 can be tuned by controlling the flake h-BN content. However, when the addition amount is excessive, the flake h-BN will stack and hinder the growth of TiO_2 nanoflake, which leads to a light shielding effect and suppresses the generation of photogenerated electron-hole pairs. The optimized addition amount of flake h-BN is 12 wt%, and the 2D TiO_2 nanoflake is uniformly attached on the surface of flake h-BN to form a novel 2D/2D h-BN/TiO_2 nanostructure composite.

In order to further investigate the growth mechanism of TiO_2 on the surface of h-BN, the morphology of the obtained h-BN and 12 wt% h-BN/TiO_2 was discussed in detail. From Fig. 2a and b, it can be observed that the morphology of the h-BN possesses graphene-like flake structure, which is advantageous for the growth of TiO_2 nanoflake and formation of h-BN/TiO_2 heterojunctions. The HRTEM image in Fig. 2c shows four parallel fringes at the edge region of the h-BN flake and the interlayer distance is 0.357 nm, which is larger than the standard value of h-BN (0.33–0.34 nm) resulting from the existence of structure defects in the obtained flake h-BN [29]. When the flake h-BN is used to construct 2D/2D h-BN/TiO_2 composites, its surface becomes rough and the flake h-BN can hardly be observed due to the dense TiO_2 nanoflakes covering on its surface as shown in Fig. 2d and

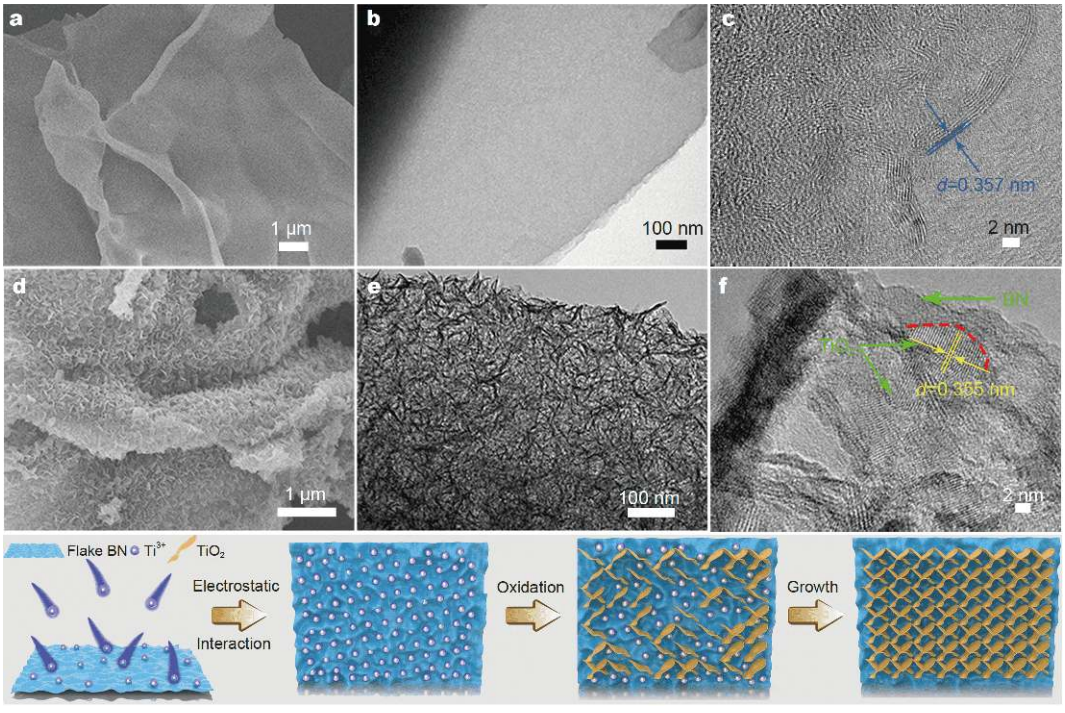

Figure 2 SEM (a) and TEM (b, c) images of the h-BN sample. SEM (d) and TEM (e, f) images of 12 wt% h-BN/TiO_2. (g) Schematic illustration of the synthetic process and growth mechanism for 2D/2D h-BN/TiO_2 composites.

e. HRTEM image in Fig. 2f demonstrates the existence of interface structure of heterojunctions (marked by red lines) between TiO_2 nanoflakes and flake h-BN. Due to the rich detects character of flake h-BN, only the (101) plane of the anatase phase TiO_2 can be observed and the fringe spacing is 0.355 nm. Based on the above results, the growth mechanism is proposed. It has been reported that the flake h-BN has an overall negative surface charge at pH above 3.2 [20], which is important for the uniform growth of TiO_2 nanoflakes on the surface of flake h-BN. As shown in Fig. 2g, when the flake of h-BN is added into the ethylene glycol solution containing $TiCl_3$, Ti^{3+} will be adsorbed on the negatively charged surface of flake h-BN by electrostatic interaction. Then the Ti^{3+} is gradually oxidized to form TiO_2 in the acidic solution during the prolonged solvothermal treatment. Meanwhile, due to the mechanical support of flake h-BN, the self-aggregated TiO_2 microspheres will scatter into nanoflakes and grow on the h-BN surface.

The surface chemical composition of the 12 wt% BN/TiO_2 composite was also investigated by XPS analysis. Fig. 3a shows that Ti 2p spectra consist of two major peaks and the binding energy of the Ti $2p_{3/2}$ peak shifts from 459.22 to 459.45 eV after introduction of the flake h-BN, indicating the close interaction between flake h-BN and TiO_2. In Fig. 3b, the O 1s spectra of TiO_2 nanoflakes are identified to two peaks with the binding energy values at 530.02 and 531.64 eV, corresponding to Ti–O and O–H bonds, respectively. However, a new peak with the binding energy at 534.1 eV corresponding to Ti–O–B bond appears in the O 1s spectra of 12 wt% BN/TiO_2 besides the same two peaks as TiO_2 [30]. Appearance of the new Ti–O–B bond further confirms the formation of heterojunctions between flake h-BN and TiO_2 nanoflakes.

The N_2 adsorption–desorption isotherms were conducted to determine the specific surface area (SSA) of the flake h-BN, pure TiO_2 and 12 wt% h-BN/TiO_2. The isotherm of the h-BN can be classified as type IV isotherm with type H4 hysteresis loop according to the IUPAC nomenclature [31], which reveals a predominant mesoporous structure (Fig. S3a). The BET model gives an SSA of 936 $m^2 g^{-1}$, and Barrett–Joyner–Halenda (BJH) calculation gives the total pore volume of 0.705 $cm^3 g^{-1}$ for h-BN, which is favor of the species adsorption. As shown in Fig. S3b, the SSA and pore volume are 151 $m^2 g^{-1}$ and 0.339 $cm^3 g^{-1}$ for pure TiO_2, and 170 $m^2 g^{-1}$ and 0.457$cm^3 g^{-1}$ for 12 wt% h-BN/TiO_2, respectively. Compared with the pure TiO_2, the SSA and pore volume of 12 wt% h-BN/TiO_2 are improved by adding the flake h-BN with high SSA, which is advantageous for improving the diffusion and adsorption capacity of organic dyes.

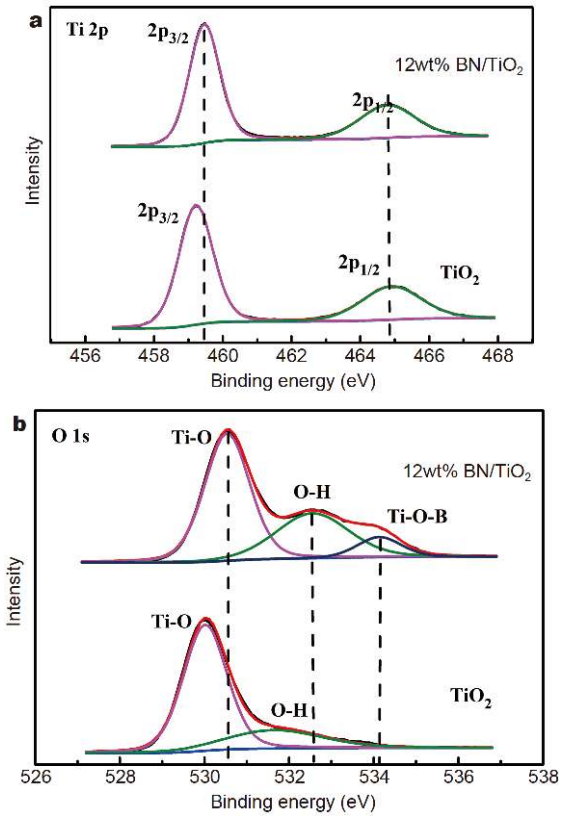

Figure 3 XPS spectra of as-prepared TiO_2 and 12 wt% BN/TiO_2 composite, (a) Ti 2p and (b) O1s.

Photocatalytic performance

The photocatalytic performance of the h-BN/TiO_2 composites was evaluated by degrading RhB under visible light irradiation. Fig. 4a shows a comparison of degradation efficiency between TiO_2 and h-BN/TiO_2. Under visible light irradiation, the synthesized TiO_2 displays a higher photocatalytic activity than commercial TiO_2 (P25), which may be attributed to the morphology difference. Compared with the P25 nanoparticles, the flake TiO_2 will offer more active sites for RhB degradation. It is well known that P25 can not absorb visible light, and thus the degradation is caused by self-photosensitized mechanism [32]. Meanwhile, it is noted that all the flake h-BN/TiO_2 composites exhibit higher photocatalytic activity than the synthesized TiO_2 and P25. The phenomenon is caused by the introduction of the flake h-BN with higher SSA which can greatly improve adsorption capacity and concentrate RhB molecules around TiO_2. Among the composites, 12 wt% h-BN/TiO_2 composite exhibits the highest photocatalytic activity and the degradation effi-

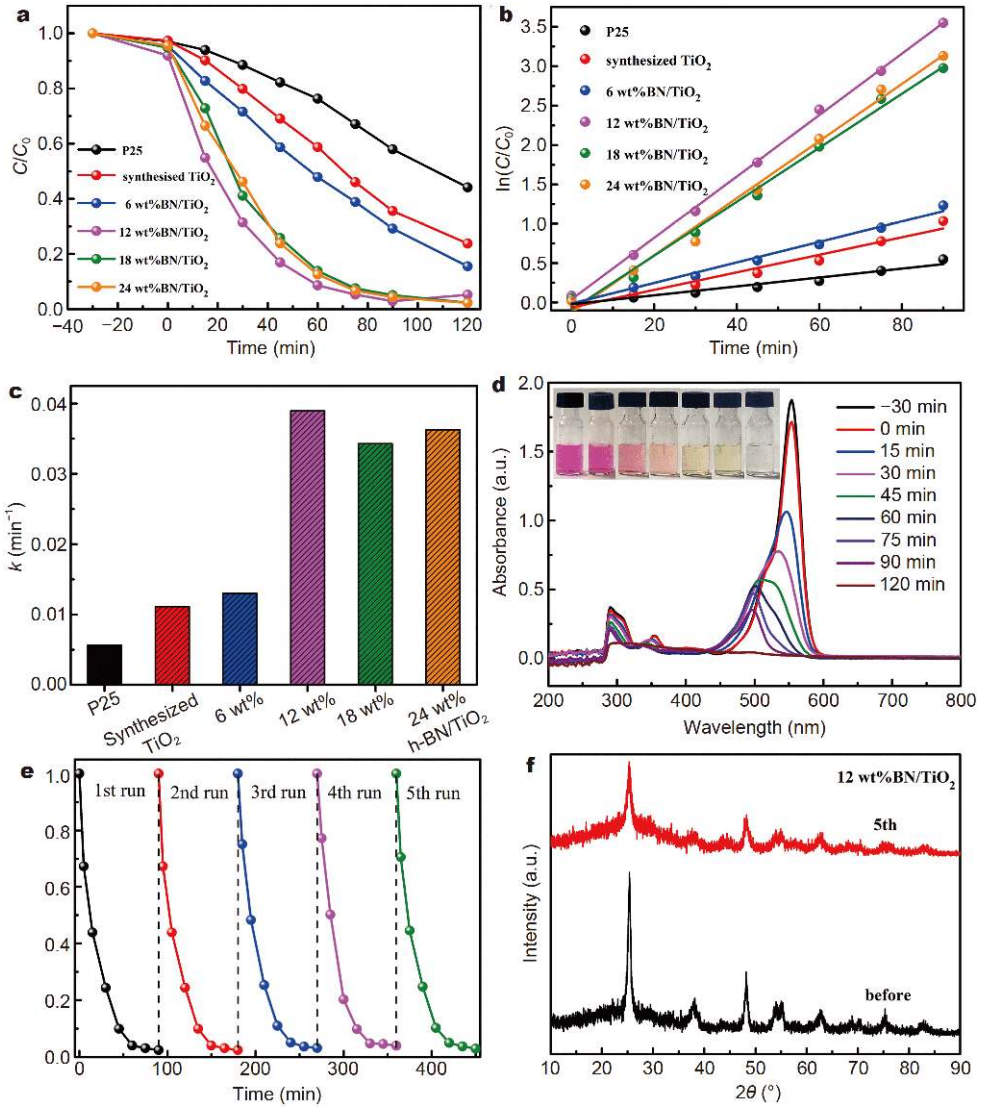

Figure 4 (a) Photodegradation rates of RhB and (b) kinetics of RhB degradation on TiO_2 and h-BN/TiO_2 samples and (c) the corresponding reaction rate constant *k*. (d) UV-vis absorption spectra and images (inset) of the aqueous RhB solution in the presence of 12 wt% h-BN/TiO_2 at different time intervals. (e) Reusability property of 12 wt% h-BN/TiO_2 composites on the photocatalytic degradation of RhB under visible light. (f) XRD patterns of the 12 wt% h-BN/TiO_2 before and after the reusability experiment.

ciency is up to 95%. For comparison, the physical mixture of BN and TiO_2 (12 wt% h-BN-TiO_2 mixture) for RhB degradation was carried out. As shown in Fig. S4, about 40% RhB is removed before light irradiation. However, only 13% RhB is removed by using the same amount of 12 wt% h-BN/TiO_2 composite. After irradiation, the composite exhibits higher photocatalytic activity than the mixture. The result indicates that immobilization of TiO_2 on the surface of flake h-BN is very effective for RhB degradation. Furthermore, phenol degradation was also performed to evaluate the photocatalytic activity and rule out the dye sensitization effect [33]. As shown in Fig. S5, 89% phenol is removed by 12 wt% h-BN/TiO_2 after 150 min, which is much higher than TiO_2 (17%). The superior photocatalytic activity of 12 wt% h-BN/TiO_2 confirms that the photocatalytic activity under visible light is responsible for the degradation of phenol rather than the dye-sensitization effect.

The kinetic behavior of the composites for degradation of RhB was further investigated under visible light irradiation. Fig. 4b shows the photocatalytic degradation of RhB following a pseudo first-order reaction: $\ln(C_0/C)=kt$,

wherein t, k, C_0 and C represent the reaction time, the apparent rate constant, the initial concentration and the concentration of RhB at given test time, respectively [34]. The kinetic constant k was calculated and presented in Fig. 4c. The increasing order of the rate constants is: 12 wt% h-BN/TiO_2 > 24 wt% h-BN/TiO_2 > 18 wt% h-BN/TiO_2 > 6 wt% h-BN/TiO_2 > synthesized TiO_2 > P25. It is worth noting that the rate constant of 12 wt% h-BN/TiO_2 is 3.5 and 6.9 times higher than that of the synthesized TiO_2 and P25, respectively, which indicates photocatalytic activity of TiO_2 is greatly improved by introducing appropriate amount of flake h-BN. Fig. 4d shows the UV-vis absorption spectra and images (inset) of the aqueous RhB solution in the presence of 12 wt% h-BN/TiO_2 at different time intervals. It can be found that the maximum absorption wavelength displays a gradual blue shift from 554 to 498 nm with increasing irradiation time, which demonstrates both de-ethylation and oxidative degradation of RhB take place and the de-ethylation process is a stepwise manner [32]. The inset of Fig. 4d shows the gradual fading of RhB color, indicating the RhB is decomposed completely. The present results are compared with those reported in the literature for dyes degradation (Table S1). It can be seen that the photocatalytic efficiency of the layered h-BN/TiO_2 composite is comparable and even higher than other BN-semiconductor systems, such as BN/Ag_3VO_4 [10], BN/WO_3 [35], BN/BiOI [36] and BN/g-C_3N_4 [37]. Notably, benefiting from the unique flake-on-flake structure, the photocatalytic performance of flake h-BN/TiO_2 composites is also superior to other BN-TiO_2 photocatalyst systems [28,38–43].

Reusability and stability

The stability and recyclability of 12 wt% h-BN/TiO_2 were investigated by the same process as mentioned above. After each run of reaction, the photocatalyst was collected for continue using. From Fig. 4e, it can be seen that the removal percentage exhibits neglected change after five cycles, indicating the excellent reusability of 12 wt% h-BN/TiO_2 composite. Fig. 4f shows the XRD patterns of the 12 wt% h-BN/TiO_2 composite before and after the recyclability experiment. No obvious change of the phase can be found except for the lower characteristic diffraction peak intensity after test, indicating the good stability of the composite under irradiation.

The photocatalytic mechanism

The optical absorption spectra of the TiO_2 and h-BN/TiO_2 composite are shown in Fig. S6. It can be seen that the absorption edge of TiO_2 is determined to be 400 nm. Compared with the pure TiO_2, h-BN/TiO_2 composites exhibit increased absorption ability in the visible light region, especially the 12 wt% BN/TiO_2, which exhibits obvious red-shift of the absorption edge and has a long and weak absorption tail covering the whole visible light region. According to the plots of Kubelka-Munk remission function (i.e., relationship of $[\alpha h\nu]^{1/2}$ *vs.* photon energy ($E_g = h\nu$), the calculated band gap values of the synthesized TiO_2 is 3.1 eV, and the value can be decreased to 2.88 eV for 12 wt% h-BN/TiO_2, indicating a narrower band gap can be obtained, which is attributed to the energy arrangement caused by the heterojunctions between TiO_2 nanoflakes and flake h-BN.

The PL emission spectra were measured with excitation light of 361 nm at room temperature. Generally, the lower PL intensity indicates lower recombination of charge carriers, resulting in higher photocatalytic activity [44]. Fig. 5a exhibits two main emission peaks centered at around 396 and 417 nm, respectively. By comparison, 12 wt% h-BN/TiO_2 exhibits the lowest intensity, demonstrating the lowest recombination rate of photogenerated electrons and holes, which is in accordance with the photocatalysis measurement (Fig. 4b). In addition, the photocurrent responses of TiO_2 and BN/TiO_2 composites were studied as shown in Fig. 5b. The h-BN/TiO_2 composites exhibit a significantly enhanced photocurrent intensity compared with the TiO_2, indicating much enhanced separation ability of electron-hole pairs after the introduction of h-BN, which results in much higher photocatalytic activity. EIS measurements were carried out as shown in Fig. 5c. The 12 wt% h-BN/TiO_2 exhibits the smallest arc radius, further indicating the lowest impedance, which can facilitate the interfacial charge-transfer process.

In order to further explore the photocatalytic mechanism of the composites, the trapping experiments were carried out to detect the main active species during the photocatalytic process. 1 mmol L^{-1} ethylenediaminetetraacetic acid disodium (EDTA-2Na), 2 mmol L^{-1} isopropanol (IPA) and 1 mmol L^{-1} benzoquinone (BQ) were chosen as scavengers for h^+, ·OH and $\cdot O_2^-$, respectively. From Fig. 5d, it can be seen that the effect of ·OH on the photocatalytic performance can be neglected, implying the ·OH does not contribute to the degradation of RhB. However, the degradation rate significantly decreases when EDTA-2Na and BQ are added, indicating h^+ and $\cdot O_2^-$ play an important role in the photocatalytic process. In addition, electron spin resonance (ESR) spin-trap technique was also carried out to further detect the active species in the photocatalytic process as shown in Fig. 5e.

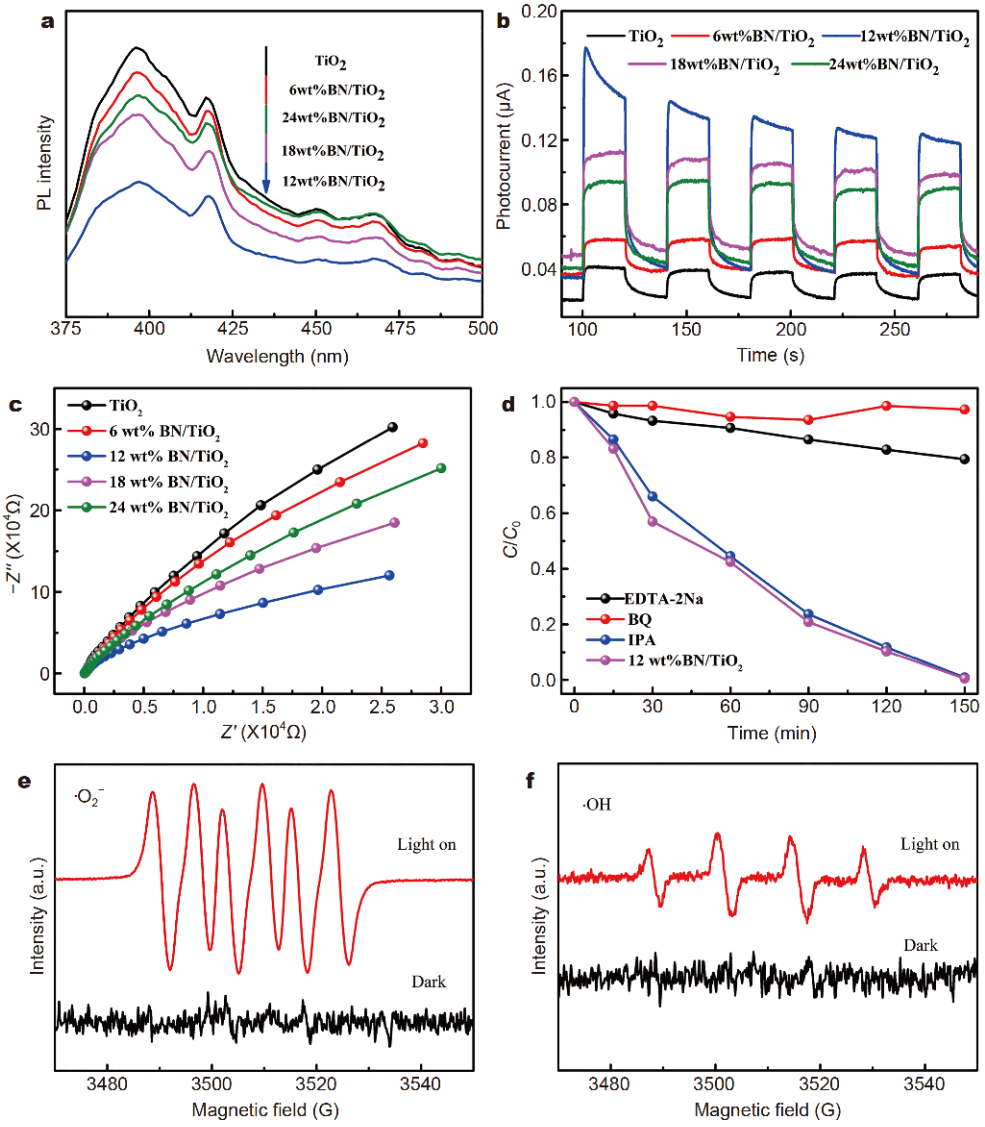

Figure 5 (a) PL emission spectra, (b) transient photocurrent responses, and (c) EIS of TiO_2 and h-BN/TiO_2 composites with different contents of flake h-BN. (d) Photocatalytic degradation of RhB on 12 wt% h-BN/TiO_2 composites in the presence of different scavengers under visible light irradiation. DMPO spin-trapping ESR spectra in (e) methanol dispersion and (f) aqueous dispersion using 12 wt% h-BN/TiO_2 under visible light irradiation.

Six strong characteristic peaks of 5,5-dimethyl-1-pyrroline-*N*-oxide (DMPO)-·O_2^- are observed in the methanol dispersion under visible light irradiation, while no signals can be found in the dark, indicating ·O_2^- radicals are indeed generated on the surface of irradiated 12 wt% h-BN/TiO_2. Interestingly, the typical weaker characteristic peaks of DMPO-·OH (Fig. 5f) were also observed, indicating ·OH can be also produced. However, from the trapping experiment, we have found that the effect of ·OH on the photocatalytic performance can be neglected. Besides, the VB value of TiO_2 after introduction of BN is not positive enough to oxidize H_2O or OH^- to ·OH (2.72 V *vs.* normal hydrogen electrode (NHE)) [45]. Thus, the generation of ·OH may be attributed to the further reduction of ·O_2^- [46]. The results further prove that RhB can be degraded by TiO_2 nanoflakes after the introduction of h-BN under visible light. The mechanism of photocatalytic enhancement was investigated by employing DFT as shown in Fig. 6. The presence of the h-BN flake in the h-BN/TiO_2 composite could effectively reduce the bandgap compared with the synthesized TiO_2 (Fig. 6a and b), which is accordance with the result of the optical ab-

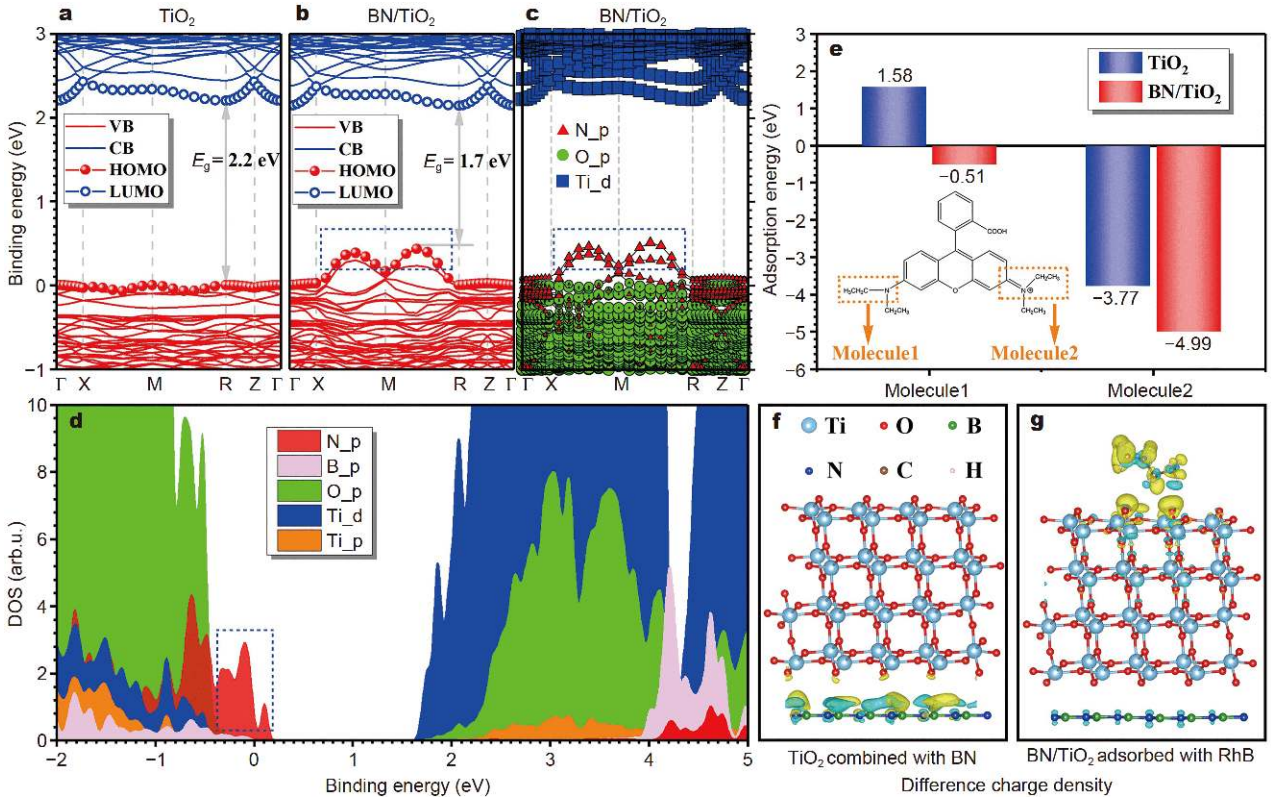

Figure 6 DFT calculation. (a, b) Band structures of TiO_2 and h-BN/TiO_2, respectively. (c, d) Contribution of N, O and Ti orbitals on band structure and density of state, respectively. (e) The adsorption energy of two kinds of molecules with ethyl groups in RhB absorbed on TiO_2 and h-BN/TiO_2. (f, g) Difference charge densities of TiO_2 combined with/without h-BN and h-BN/TiO_2 adsorbed with/without RhB.

sorption spectra. The reduction of bandgap is caused by the upshift of VBM contributed by the N-p orbital of h-BN (as shown in the two peaks in Fig. 6b and c labeled by dashed boxes). Besides, CB and VB derive mainly from Ti-d and N-p orbitals, which could also be obtained from DOS in Fig. 6d. The state in VBM labeled by dashed box consists of N-p orbital, which lifts the VBM and reduces the bandgap. Furthermore, the band of the highest occupied molecular orbital (HOMO) of h-BN/TiO_2 is much more bent than that of TiO_2 (Fig. 6a and b), clarifying that the hole of h-BN/TiO_2 has much lighter effective mass than that of TiO_2. The hole effective mass of TiO_2 and h-BN/TiO_2 is 0.57 and 0.12 m_0 (m_0 is the rest mass of electron). Therefore, the addition of h-BN could increase the hole carrier mobility, which is beneficial for the oxidation of RhB. In addition, two different parts of the RhB with ethyl group were chosen as the adsorbed molecules. Fig. 6e shows molecule 2 has more negative adsorption energy, i.e., easier to be adsorbed, and h-BN/TiO_2 has better adsorption ability than TiO_2. Therefore, the flake h-BN could increase the adsorption of RhB around the TiO_2 surface. The difference charge densities were also calculated to observe the charge transfer (Fig. 6f). There is large charge accumulation and charge depletion around N and B atoms, respectively, which will form the strong p-p coupling between the N-p and B-p orbitals, leading to the more bent HOMO (Fig. 6b). Meanwhile, there is also more or less charge accumulation around the O atoms close to h-BN, indicating the addition of h-BN can contribute electrons to TiO_2. When molecule 2 is adsorbed on the surface of h-BN/TiO_2, there is a large charge accumulation on the surface of TiO_2, which leads to the electronic loss of molecule 2 and causes the de-ethylation process. DFT calculation further proves that the addition of h-BN into TiO_2 can indeed enhance the photocatalytic performance.

Based on the above results, the possible mechanism of the h-BN/TiO_2 is proposed as shown in Fig. 7. The CB and VB edge potentials of the synthesized TiO_2 were theoretically speculated by means of atom's Mulliken electronegativity: $E_{CB} = X - E_C - 0.5E_g$; $E_{VB} = E_g + E_{CB}$, where X represents the absolute electronegativity of the

semiconductor; E_C and E_g are the energy of free electrons on hydrogen scale (~4.5 eV) and band gap, respectively [47]. The band edge potentials of CB and VB are −0.19 and 2.91 eV, respectively, as shown in Fig. 7. The redox potentials of RhB and excited RhB* are 0.95 and −1.42 eV *vs.* NHE, respectively [48]. It is much easier for RhB to be oxidized at its excited state. Under illumination, due to the upshift of VB after the introduction of h-BN, electrons in VB can be excited to CB, so holes are left on the VB. At the same time, RhB can be excited to form excited states (RhB*), leading to electrons with injection from the adsorbed RhB* species to the TiO_2 CB [49]. Due to the introduction of h-BN with high SSA, more adsorbed RhB* species concentrate on the surface of TiO_2. So, more electrons transfer to CB of TiO_2. In addition, the reduction potential of $O_2/\cdot O_2^-$ is −0.046 eV *vs.* NHE [13]. Thus, the CB value of TiO_2 is negative enough to reduce the adsorbed O_2 to $\cdot O_2^-$, which directly participate in the oxidation reaction. Importantly, both the flake-on-flake structure and the negatively charged h-BN will effectively promote h^+ transfer from the inner of TiO_2 to its surface, and further improve the separation of photogenerated electron and hole pairs. Besides, Fig. 7 shows that the VB value of TiO_2 is positive enough to oxidize RhB. That is to say that the h-BN flake works as a successive catalyst support material and plays a role of preventing the recombination of electrons and holes produced in TiO_2 nanoflakes, following the synergetic catalytic effect of type II proposed in our previous work [50]. The possible reaction process for the decomposition of RhB is given in equations (3–9):

$$TiO_2 + h\nu \rightarrow TiO_2(e^- + h^+), \quad (3)$$

$$RhB + h\nu \rightarrow RhB^*, \quad (4)$$

$$RhB^* + TiO_2 \rightarrow RhB^+ + TiO_2(e^-), \quad (5)$$

$$TiO_2(e^- + h^+) + BN \rightarrow TiO_2(e^-) + BN(h^+), \quad (6)$$

$$TiO_2(e^-) + O_2 \rightarrow TiO_2 + \cdot O_2^-, \quad (7)$$

$$\cdot O_2^- + RhB^+/RhB \rightarrow \text{degradation}\ldots\text{products}, \quad (8)$$

$$BN(h^+) + RhB^+/RhB \rightarrow \text{degradation}\ldots\text{products}. \quad (9)$$

CONCLUSIONS

A novel 2D/2D h-BN/TiO_2 composite photocatalyst with flake-on-flake nanostructure was successfully synthesized by a solvothermal method with *in situ* growth technology. As expected, the introduction of the flake h-BN can greatly improve the photocatalytic performance of the obtained composites. Especially for the 12 wt% h-BN/TiO_2 composite, a high photocatalytic efficiency up to 95% for the degradation RhB under visible light has been obtained, and its rate constant is 3.5 and 6.9 times higher than that of the synthesized TiO_2 and P25, respectively. Moreover, the 2D/2D h-BN/TiO_2 composite exhibits excellent cycling stability and reusability. DFT calculation further proves that the addition of h-BN into TiO_2 can indeed enhance the photocatalytic performance of composites. A synergetic catalytic mechanism has been formed on the heterojunctions between h-BN and TiO_2 during the degradation of RhB, in which the ability of visible light absorption is improved on one hand, and on the other hand the photosensitized RhB can increase the degradation rate of RhB by injecting electrons from the adsorbed RhB* species to the TiO_2 CB to generate more active oxygen species $\cdot O_2^-$. Meanwhile, not only the negatively charged h-BN improve the separation of photogenerated electron and hole pairs, but its larger specific surface area can also concentrate the RhB molecules around TiO_2 to improve the kinetics. This work not only develops a new multifunctional h-BN/TiO_2 composite as photocatalysts under visible light irradiation, but also provides a new way to design advanced composite photocatalysts.

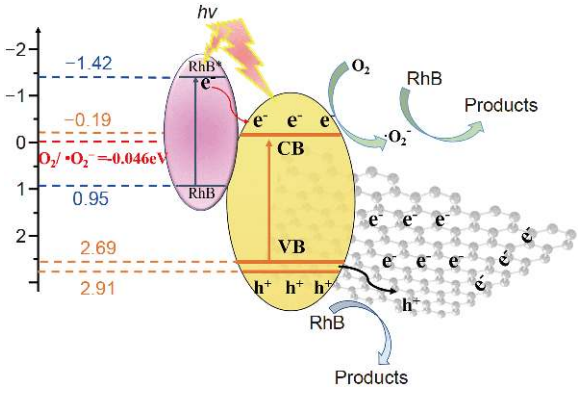

Figure 7 Photocatalytic degradation mechanism of h-BN/TiO_2 composite.

Received 21 June 2019; accepted 5 September 2019; published online 25 October 2019

1 Shahabuddin S, Khanam R, Khalid M, *et al.* Synthesis of 2D boron nitride doped polyaniline hybrid nanocomposites for photocatalytic degradation of carcinogenic dyes from aqueous solution. Arabian J Chem, 2018, 11: 1000–1016
2 Liu W, Liu Z, Wang G, *et al.* Carbon coated Au/TiO_2 mesoporous microspheres: a novel selective photocatalyst. Sci China Mater, 2017, 60: 438–448
3 Tan Y, Liu M, Wei D. A simple green approach to synthesis of sub-100 nm carbon spheres as template for TiO_2 hollow nanospheres with enhanced photocatalytic activities. Sci China Mater, 2018, 61:

869–877
4 Fan Y, Hu G, Yu S, *et al.* Recent advances in TiO_2 nanoarrays/graphene for water treatment and energy conversion/storage. Sci China Mater, 2019, 62: 325–340
5 Yin W, Bai S, Zhong Y, *et al.* Direct generation of fine Bi_2WO_6 nanocrystals on g-C_3N_4 nanosheets for enhanced photocatalytic activity. ChemNanoMat, 2016, 2: 732–738
6 Bera R, Kundu S, Patra A. 2D hybrid nanostructure of reduced graphene oxide–CdS nanosheet for enhanced photocatalysis. ACS Appl Mater Interfaces, 2015, 7: 13251–13259
7 Wang S, Luo H, Xu X, *et al.* Enhanced organic dye removal of porous BN fibers supported Ta_3N_5 nanoparticles under visible light irradiation. Surfs Interfaces, 2016, 5: 39–46
8 Xu H, Wu Z, Ding M, *et al.* Microwave-assisted synthesis of flower-like BN/BiOCl composites for photocatalytic Cr(VI) reduction upon visible-light irradiation. Mater Des, 2017, 114: 129–138
9 Ide Y, Liu F, Zhang J, *et al.* Hybridization of Au nanoparticle-loaded TiO_2 with BN nanosheets for efficient solar-driven photocatalysis. J Mater Chem A, 2014, 2: 4150–4156
10 Lv X, Wang J, Yan Z, *et al.* Design of 3D h-BN architecture as Ag_3VO_4 enhanced photocatalysis stabilizer and promoter. J Mol Catal A-Chem, 2016, 418-419: 146–153
11 Wang M, Li M, Xu L, *et al.* High yield synthesis of novel boron nitride submicro-boxes and their photocatalytic application under visible light irradiation. Catal Sci Technol, 2011, 1: 1159–1165
12 Wang J, Shen J, Fan D, *et al.* BN nanosheet: an efficient carriers transfer promoter and stabilizer to enhance the photocatalytic performance of Ag_2CO_3. Mater Lett, 2015, 147: 8–11
13 Ding S, Mao D, Yang S, *et al.* Graphene-analogue h-BN coupled Bi-rich $Bi_4O_5Br_2$ layered microspheres for enhanced visible-light photocatalytic activity and mechanism insight. Appl Catal B-Environ, 2017, 210: 386–399
14 Ma F, Zhao G, Li C, *et al.* Fabrication of CdS/BNNSs nanocomposites with broadband solar absorption for efficient photocatalytic hydrogen evolution. CrystEngComm, 2016, 18: 631–637
15 Chen J, Zhu J, Da Z, *et al.* Improving the photocatalytic activity and stability of graphene-like BN/AgBr composites. Appl Surf Sci, 2014, 313: 1–9
16 Ji M, Xia J, Di J, *et al.* Graphene-like boron nitride induced accelerated charge transfer for boosting the photocatalytic behavior of $Bi_4O_5I_2$ towards bisphenol A removal. Chem Eng J, 2018, 331: 355–363
17 Zhou C, Lai C, Zhang C, *et al.* Semiconductor/boron nitride composites: synthesis, properties, and photocatalysis applications. Appl Catal B-Environ, 2018, 238: 6–18
18 Zhang K, Fujitsuka M, Du Y, *et al.* 2D/2D heterostructured CdS/WS_2 with efficient charge separation improving H_2 evolution under visible light irradiation. ACS Appl Mater Interfaces, 2018, 10: 20458–20466
19 Ye M, Gong J, Lai Y, *et al.* High-efficiency photoelectrocatalytic hydrogen generation enabled by palladium quantum dots-sensitized TiO_2 nanotube arrays. J Am Chem Soc, 2012, 134: 15720–15723
20 Li Q, Huo C, Yi K, *et al.* Preparation of flake hexagonal BN and its application in electrochemical detection of ascorbic acid, dopamine and uric acid. Sens Actuat B-Chem, 2018, 260: 346–356
21 Fu X, Hu Y, Zhang T, *et al.* The role of ball milled h-BN in the enhanced photocatalytic activity: A study based on the model of ZnO. Appl Surf Sci, 2013, 280: 828–835
22 Perdew JP, Burke K, Ernzerhof M. Generalized gradient approximation made simple. Phys Rev Lett, 1996, 77: 3865–3868
23 Kresse G, Furthmüller J. Efficient iterative schemes for *ab initio* total-energy calculations using a plane-wave basis set. Phys Rev B, 1996, 54: 11169–11186
24 Kresse G, Joubert D. From ultrasoft pseudopotentials to the projector augmented-wave method. Phys Rev B, 1999, 59: 1758–1775
25 Dudarev SL, Botton GA, Savrasov SY, *et al.* Electron-energy-loss spectra and the structural stability of nickel oxide: An LSDA+U study. Phys Rev B, 1998, 57: 1505–1509
26 Zhang J, Peng C, Wang H, *et al.* Identifying the role of photogenerated holes in photocatalytic methanol dissociation on rutile TiO_2 (110). ACS Catal, 2017, 7: 2374–2380
27 Hu H, Yu L, Gao X, *et al.* Hierarchical tubular structures constructed from ultrathin TiO_2 (B) nanosheets for highly reversible lithium storage. Energy Environ Sci, 2015, 8: 1480–1483
28 Liu D, Zhang M, Xie W, *et al.* Porous BN/TiO_2 hybrid nanosheets as highly efficient visible-light-driven photocatalysts. Appl Catal B-Environ, 2017, 207: 72–78
29 Zhang X, Lian G, Zhang S, *et al.* Boron nitride nanocarpets: controllable synthesis and their adsorption performance to organic pollutants. CrystEngComm, 2012, 14: 4670–4676
30 Chen D, Yang D, Wang Q, *et al.* Effects of boron doping on photocatalytic activity and microstructure of titanium dioxide nanoparticles. Ind Eng Chem Res, 2006, 45: 4110–4116
31 Li J, Huang Y, Liu Z, *et al.* Chemical activation of boron nitride fibers for improved cationic dye removal performance. J Mater Chem A, 2015, 3: 8185–8193
32 Wu T, Liu G, Zhao J, *et al.* Photoassisted degradation of dye pollutants. V. Self-photosensitized oxidative transformation of rhodamine B under visible light irradiation in aqueous TiO_2 dispersions. J Phys Chem B, 1998, 102: 5845–5851
33 Long M, Cai W, Cai J, *et al.* Efficient photocatalytic degradation of phenol over Co_3O_4/$BiVO_4$ composite under visible light irradiation. J Phys Chem B, 2006, 110: 20211–20216
34 Xu J, Meng W, Zhang Y, *et al.* Photocatalytic degradation of tetrabromobisphenol A by mesoporous BiOBr: efficacy, products and pathway. Appl Catal B-Environ, 2011, 107: 355–362
35 Xu H, Liu L, Song Y, *et al.* BN nanosheets modified WO_3 photocatalysts for enhancing photocatalytic properties under visible light irradiation. J Alloys Compd, 2016, 660: 48–54
36 Liu D, Jiang Z, Zhu C, *et al.* Graphene-analogue BN-modified microspherical BiOI photocatalysts driven by visible light. Dalton Trans, 2016, 45: 2505–2516
37 Gu J, Yan J, Chen Z, *et al.* Construction and preparation of novel 2D metal-free few-layer BN modified graphene-like g-C_3N_4 with enhanced photocatalytic performance. Dalton Trans, 2017, 46: 11250–11258
38 Nasr M, Viter R, Eid C, *et al.* Enhanced photocatalytic performance of novel electrospun BN/TiO_2 composite nanofibers. New J Chem, 2017, 41: 81–89
39 Singh B, kaur G, Singh P, *et al.* Nanostructured BN–TiO_2 composite with ultra-high photocatalytic activity. New J Chem, 2017, 41: 11640–11646
40 Si H, Lian G, Wang J, *et al.* Synthesis of few-atomic-layer BN hollow nanospheres and their applications as nanocontainers and catalyst support materials. ACS Appl Mater Interfaces, 2016, 8: 1578–1582
41 Xie W, Zhang M, Liu D, *et al.* Reactive yellow 161 decolorization by TiO_2/porous boron nitride nanosheet composites in cotton

dyeing effluent. ACS Sustain Chem Eng, 2016, 5: 1392–1399
42 Fu X, Hu Y, Yang Y, *et al.* Ball milled h-BN: an efficient holes transfer promoter to enhance the photocatalytic performance of TiO_2. J Hazard Mater, 2013, 244-245: 102–110
43 Liu D, Cui W, Lin J, *et al.* A novel $TiO_{2-x}N_x$/BN composite photocatalyst: Synthesis, characterization and enhanced photocatalytic activity for rhodamine B degradation under visible light. Catal Commun, 2014, 57: 9–13
44 Zhou M, Yu J, Liu S, *et al.* Effects of calcination temperatures on photocatalytic activity of SnO_2/TiO_2 composite films prepared by an EPD method. J Hazard Mater, 2008, 154: 1141–1148
45 Li G, Wong KH, Zhang X, *et al.* Degradation of acid orange 7 using magnetic AgBr under visible light: the roles of oxidizing species. Chemosphere, 2009, 76: 1185–1191
46 Jiang L, Yuan X, Zeng G, *et al.* Metal-free efficient photocatalyst for stable visible-light photocatalytic degradation of refractory pollutant. Appl Catal B-Environ, 2018, 221: 715–725
47 Meng S, Ning X, Zhang T, *et al.* What is the transfer mechanism of photogenerated carriers for the nanocomposite photocatalyst Ag_3PO_4/g-C_3N_4, band–band transfer or a direct Z-scheme? Phys Chem Chem Phys, 2015, 17: 11577–11585
48 Fang Z, Li Q, Su L, *et al.* Efficient synergy of photocatalysis and adsorption of hexavalent chromium and rhodamine B over Al_4SiC_4/rGO hybrid photocatalyst under visible-light irradiation. Appl Catal B-Environ, 2019, 241: 548–560
49 Wang Y, Wang H, Xu A, *et al.* Facile synthesis of Ag_3PO_4 modified with GQDs composites with enhanced visible-light photocatalytic activity. J Mater Sci-Mater Electron, 2018, 29: 16691–16701
50 Shi J. On the synergetic catalytic effect in heterogeneous nanocomposite catalysts. Chem Rev, 2013, 113: 2139–2181

Acknowledgements This work was supported by the National Natural Science Foundation for Excellent Young Scholars of China (51522402), the National Postdoctoral Program for Innovative Talents (BX20180034), the Fundamental Research Funds for the Central Universities (FRF-TP-18-045A1), and China Postdoctoral Science Foundation (2018M641192).

Author contributions Hou X, Chen J, Liang T and Shi J supervised the experiment. Li Q and Yang T proposed the idea. Li Q designed and performed the experiment and wrote the paper. Fang Z contributed to the DFT calculations. Cui X and Hou X revised the paper. All authors contributed to the general discussion.

Conflict of interest The authors declare that they have no conflict of interest.

Supplementary information Supporting data are available in the online version of the paper.

Qun Li is currently studying for her PhD degree in the University of Science and Technology Beijing, China. Her research focuses on the preparation of materials, electrochemical and adsorption application

Xinmei Hou received her Bachelor's and Master's degree from Zhengzhou University, and got her PhD degree from the University of Science and Technology Beijing in 2009. Now she is a full professor of University of Science and Technology Beijing. Her research interests include the preparation of high performance ceramics, high temperature properties and functional applications in such fields of electrochemistry and environment.

Xiangzhi Cui received her PhD degree in 2009 from Shanghai Institute of Ceramics, Chinese Academy of Sciences, and has been working at the institute since then. Her main research interest includes the structural design and synthesis of mesostructured nanocomposites, and the catalytic performances of the materials for applications in fuel cells and environmental protection.

层状h-BN/TiO_2异质结构的构建及其协同光催化效应探讨

李群[1], 侯新梅[1*], 方志[1], 杨涛[1], 陈俊红[2], 崔香枝[3*], 梁彤祥[4], 施剑林[3]

摘要 本文采用溶剂热法将纳米二氧化钛(TiO_2)片固定在六方氮化硼(h-BN)片表面, 制备了一种新型层状h-BN/TiO_2复合光催化剂. 由于其独特的异质结构, 合成的复合材料对罗丹明B(RhB)降解的光催化性能得到了提高, 其中12 wt% h-BN/TiO_2的降解率分别比合成的TiO_2和P25高3.5倍和6.9倍, 同时具有良好的循环稳定性. 此外, 第一原理计算揭示了TiO_2与h-BN片之间的协同催化作用, 发现h-BN的引入对h-BN/TiO_2复合材料的光催化性能有显著提高.

